Chemical Engineering Journal 93 (2003) 103–112

Chemical Engineering Journal

www.elsevier.com/locate/cej

CFD models for methanol synthesis three-phase reactors: reactor optimization

Isaac K. Gamwo [a,*], John S. Halow [a], Dimitri Gidaspow [b], Reza Mostofi [b]

[a] *National Energy Technology Laboratory, United States Department of Energy, P.O. Box 10940, Pittsburgh, PA 15236-0940, USA*
[b] *Department of Chemical and Environmental Engineering, Illinois Institute of Technology, Chicago, IL 60616, USA*

Received 30 November 2001; accepted 23 July 2002

Abstract

Two Computational Fluid Dynamics (CFD) models have been developed for slurry bubble columns. The first model is based on the kinetic theory of granular flow with a measured restitution coefficient in a slurry bubble column. The model was used to predict Air Products/DOE La Porte reactor's slurry height, gas hold-up and the rate of methanol production. It showed an unfavorable high solids concentration at the bottom of the reactor. The second model with a catalyst viscosity as an input has computed the measured flow patterns and Reynolds stresses in agreement with measurements in a laboratory slurry bubble column.

Here, we have rearranged the heat exchangers in the La Porte unit and constructed a CFD model for a baffled reactor that has a higher concentration of the catalyst in the upper portion of the reactor. In this arrangement, the conversion to products is higher than in the La Porte unit, because there is more catalyst in the region of decreased reactant concentration. The baffled arrangement of the heat exchangers prevents the mixing of the catalyst from the upper stage, allowing continued operation of the reactor with a high concentration in the upper stage. Thus, an optimum catalyst concentration is maintained during the course of the production of the liquid fuels.

Keywords: CFD models; Slurry bubble column reactors; Optimum catalyst distribution

1. Introduction

Slurry bubble column reactors (SBCRs) have recently become competitive with traditional tubular fixed-bed reactors for converting syn-gas into liquid fuels due to several advantages, including better temperature control and mass transfer, lower operating and capital costs. The design of these reactors require, among other things, precise knowledge of the kinetics, hydrodynamics, and heat as well as mass transfer characteristics.

A decade ago, Stiegel of PETC [1] published a comprehensive review of DOE research in Fischer–Tropsch (F–T) technology. It described the advantages of the slurry-phase reactor over the fixed bed reactor, which are excellent heat and mass transfer and the ability to easily replace the catalyst due to its fluid-like properties, when properly prepared. Catalysts for Fischer–Tropsch (F–T) processes were reviewed by Srivastava et al. [2].

Early slurry bubble column reactor (SBCR) models were reviewed by Ramachandran and Chaudhari [3], Deckwer [4] and by Fan [5]. They require hold-up correlations as an input and do not compute flow patterns. The most complete of these models applied to the F–T conversion of synthesis gas in a SBCR is that of Prakash and Bendale [6]. They sized commercial SBCR for the US Department of Energy. They gave syn-gas conversion and production as a function of temperature, pressure and space velocity. Input parameters with considerable uncertainty that influenced production rates were the gas hold-up, the mass transfer coefficient and the dispersion coefficient. Van der Laan et al. [7] extended such a model to compute product distribution using a product selectivity model. Degaleesan et al. [8] measured dispersion coefficients needed as an input into such a model. The problem with this approach is that the dispersion coefficients are not constant. They are a function of the local hydrodynamics. Ten years ago, Tarmy and Coulaloglu [9] stated that there exists no hydrodynamic models in the open literature.

The multiphase CFD approach does not require dispersion coefficients as an input. Hold-up and flow patterns are computed. Pan et al. [10] is using the CFD approach to compute gas–liquid flow using Los Alamos CFDLIB code with a viscosity as an input and are working on liquid–solid flow [11], but have no models or codes for gas–liquid–solid flow. Luo et al. [12] built a unique high-pressure bubble column and developed PIV and other techniques useful for multiphase

* Corresponding author. Tel.: +1-412-386-6537; fax: +1-412-386-5936.
E-mail address: gamwo@netl.doe.gov (I.K. Gamwo).

1385-8947/02/$ – see front matter
PII: S1385-8947(02)00192-4

Nomenclature

C_D	drag coefficient
d_k	mean diameter of solid particle
e_k	restitution coefficient of phase k
f_j	fugacity of j
$\boldsymbol{g}$	gravity acceleration
g_0	radial distribution function of phase k
$[\boldsymbol{I}]$	unit tensor
K_{eq}	reaction equilibrium constant
K_r	reaction kinetic coefficient
M^j	molecular weight of j
N	total number of species
P_k	pressure of phase k
r_{ik}	rate of ith reaction in phase k
$\tilde{R}$	universal gas constant
Re_k	Reynolds number based on d_k
T	thermal temperature
$\boldsymbol{T}_k$	shear stress of phase k
u	x-component of velocity
U	superficial velocity
v	y-component of velocity
$\boldsymbol{v}$	velocity vector
y_g^j	weight fraction

Greek letters

α^j	stoichiometric coefficient
β	frictional coefficient between phases k and l
ε_k	volume fraction of phase k
γ	collisional energy dissipation
κ_s	conductivity of fluctuating energy
μ_k	viscosity of phase k
θ	granular temperature
ρ_k	density of phase k
ξ_k	bulk viscosity

Subscripts

g, l, s	gas, liquid, solid, respectively
i	ith reaction
k	gas, liquid, solid (g, l, s)

Superscript

j	species

measurements. Mitra-Majumdar et al. [13] and Bohn [14] are using the k-epsilon turbulence model in their CFD approach. This model has too many unknown parameters when applied to multiphase flow. The kind of model used by Pan et al. [10] computed the Reynolds stresses in agreement with measurements done in Fan's laboratory. In Matonis et al. [15], we show our capability to compute turbulence in a slurry bubble column in the churn-turbulent regime in agreement with our measurements. In Matonis et al. [15], turbulence and hydrodynamics are computed with the measured particle viscosity as an input. Wu and Gidaspow [16] used a kinetic theory model. The catalyst viscosity is automatically computed. Here, the more advanced model of Wu and Gidaspow [16] is used to explore novel reactor designs. The major change in the computation involves the simulation of the whole reactor. To save computation time, Wu and Gidaspow [16] simulated half the reactor only, obtaining complete symmetry. Later research showed that such an assumption could sometimes produce inaccurate results.

2. Slurry bubble column experiment

Operation of some slurry bubble column reactors often [17] involves recirculation of the liquid. To study such systems, a rectangular bed was constructed from transparent acrylic (Plexiglas) sheets at IIT [18]. This material was used to facilitate visual observation and video recording of the bed performance such as gas bubbling and coalescence, and the mixing and segregation of solids. The bed height was 213.36 cm and cross-section was 30.48 cm × 5.08 cm. A centrifugal pump was connected to the bottom of the bed by a 1.0 in. (2.54 cm) diameter stainless steel pipe. Gas injection nozzles from an air compressor were connected to the sides of the bed. Liquid was stored in a 55 gal storage tank and recycled back to the bed. Fig. 1a shows a schematic diagram of the experimental set-up.

The liquid and gas distributors were located at the bottom of the bed. The liquid was distributed by two perforated Plexiglas plates with many 0.28 cm diameter holes. They were placed at 35.6 and 50.8 cm above the bottom of the bed, respectively; 0.25 cm size glass bead particles distributed the liquid, as shown in Fig. 1a. The gas distributor consisted of six staggered porous tubes of 15.24 cm length and 0.28 cm diameter. The fine pores of the porous tubes had a mean diameter of 42 μm. The porous tubes were placed at the bottom of the bed, just below the top perforated plate. Air and water were used as the gas and liquid, respectively in this experiment. Ballotini (leaded glass beads) with an average diameter of 0.8 mm and a density of 2.94 g/cm^3 were used as the solids. Fig. 1b shows a picture of the experiment for $U_g = 3.36$ and $U_l = 2.24$ cm/s. Two distinct bubbles are seen in the middle of the bed, as two bright regions.

The two-fluid model with solids viscosity as an input was used by Matonis et al. [15] to simulate this system. Fig. 2 shows a comparison of two- and three-dimensional simulations to the experiment. The peaks in velocities correspond to motion of the two bubbles shown in Fig. 1b. The computed turbulent particle kinetic energy (3/2 granular temperature) is shown in Fig. 3. The computed turbulent kinetic energy is nearly constant due to the fact that the particle concentration is nearly uniform in this system.

3. Hydrodynamic model

A transient, reactive, two-dimensional model for multiphase flow was developed [16]. The hydrodynamic model

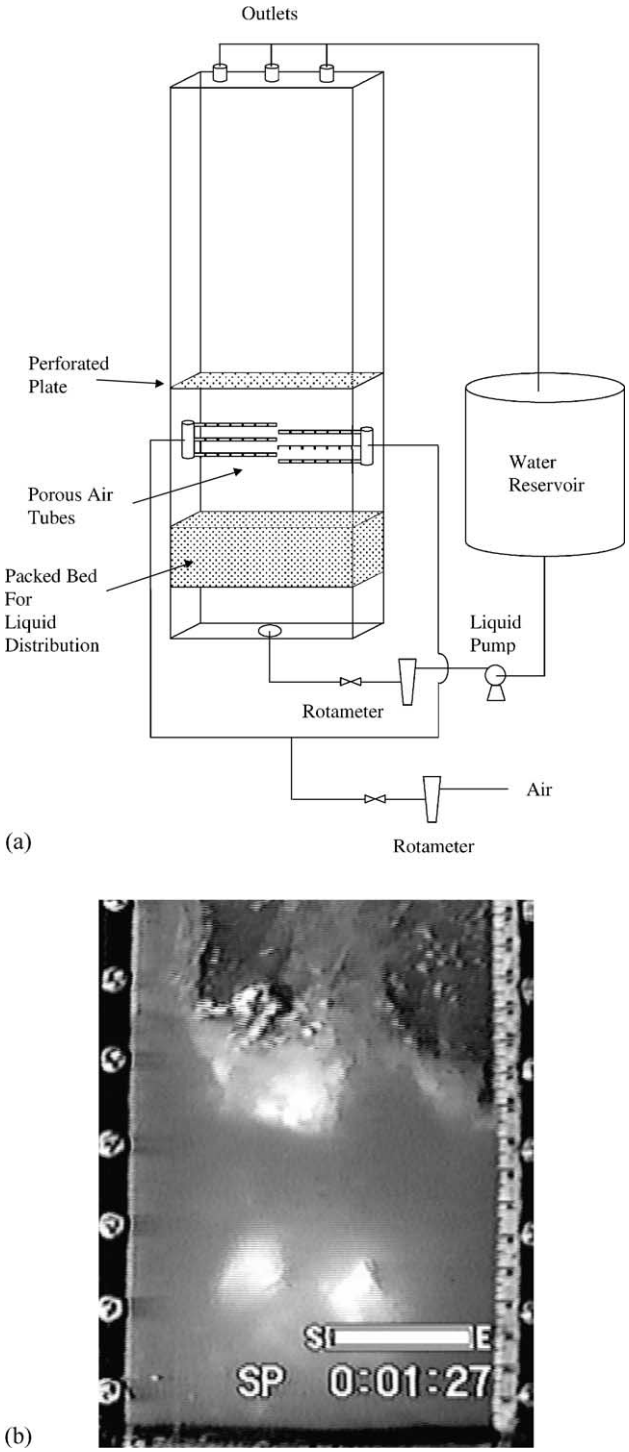

Fig. 1. (a) Schematic diagram of IIT slurry bubble column. (b) IIT slurry bubble column with liquid recirculation.

uses the principle of mass conservation and momentum balance for each phase.

The modeling approach is similar to that of Soo [19] for multiphase flow and of Jackson [20] for fluidization. The equations are similar to Bowen's [21] balance laws for multi-component mixtures. The principal difference is the

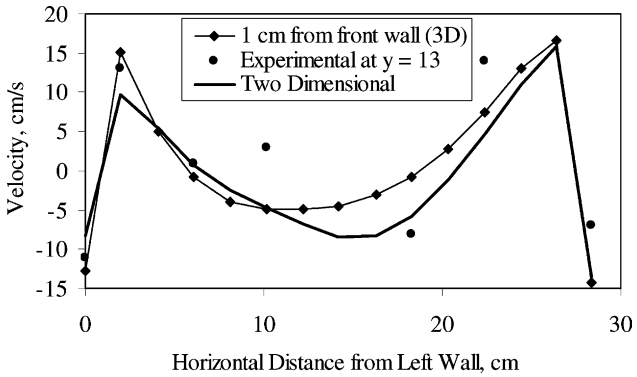

Fig. 2. A comparison of two- and three-dimensional particle velocities to PIV measurements [15].

appearance of the volume fraction of phase "k" denoted by ε_k. The fluid pressure, P, is in the gas (continuous) phase. For gas–solid fluidized beds, Bouillard and Gidaspow [22] have shown that this set of equations produces essentially the same numerical answers for fluidization as did the earlier conditionally stable model, which has the fluid pressure in both the gas and the solids phases, and is referred to as model B [23]. In this model, the drag and the stress relations were altered to satisfy Archimedes' buoyancy principle and Darcy's law, as illustrated by Jayaswal [24]. Note in the continuous phase momentum equation, no volume fraction is put into the gravity term, while the dispersed phases momentum balances contain the buoyancy term.

This is a generalization of model B for gas–solid systems as discussed by Gidaspow [25] in Section 2.4. For the solid phase P_k, consists of the static normal stress and dynamic stress, called the solids pressure, which arises due to the collision of the particles, as explained by Gamwo et al. [26].

This model is unconditionally well-posed, i.e. the characteristics are real and distinct for one-dimensional transient flow. It does not require the presence of solids pressure for stability and well-posedness. The numerical method is an extension of Harlow and Amsden's [27] method, which was

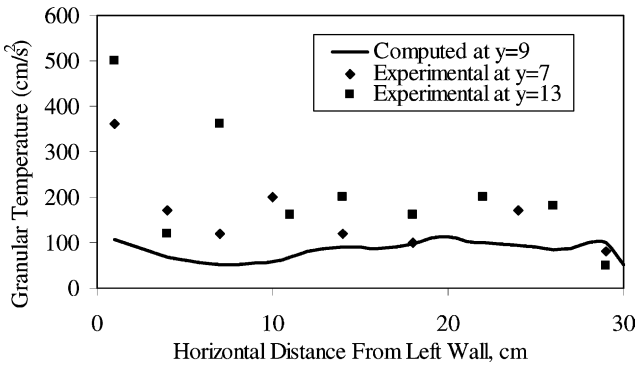

Fig. 3. Comparison of experimental granular temperatures at different bed heights and granular temperature like average normal Reynolds stresses (note: splashing on left wall, Fig. 1b, possibly leading to higher granular temperatures near the left wall).

subsequently used in the K-FIX program [28]. The present program was developed from Jayaswal's two-dimensional MICE program [24]; which originated from the K-FIX program. To obtain the numerical solution, the non-uniform computational mesh is used in finite-differencing the equations based on the ICE, implicit Eulerian method [24,28] with appropriate initial and boundary conditions. Stewart and Wendroff [29] have critically reviewed the ICE algorithm and related staggered mesh conservative schemes. The scalar variables are located at the cell center and the vector variables at the cell boundaries. The momentum equation is solved using a staggered mesh, while the continuity equation is solved using a donor cell method. For a highly non-linear non-isothermal reactive flow it may be necessary to use a different numerical approach [30].

The partial differential equations used to describe the reactive three-phase flow are the continuity for each phase, the separate phase momentum equations, the fluctuating energy equation for particles and finally the species balances for the gas phase. The variables to be computed are the volume fractions, ε_g, ε_l, ε_s, the gas phase pressure P_g and species concentrations, and the three phases horizontal, x-direction, and vertical, y-direction velocity, components, u_g, u_l, u_s and v_g, v_l, v_s. Due to uncertainties of mass transfer coefficients, mass transfer in the liquid phase was not included. The gradient of pressure is in the continuous phase only. This leads to an unconditionally well-posed problem, as discussed in detail by Gidaspow [25] and Lyczkowski et al. [31]. This hydrodynamic model is based on the kinetic theory and is shown in the following paragraphs.

Continuity equations for gas, liquid and solids (k = g, l, s):

$$\frac{\partial}{\partial t}(\varepsilon_k \rho_k) + \nabla \cdot (\varepsilon_k \rho_k \boldsymbol{v}_k) = 0 \tag{1}$$

Conservation of phase-volume fraction:

$$\varepsilon_g + \varepsilon_l + \varepsilon_s = 1 \tag{2}$$

The standard multiphase momentum balance is (k = g, l, s):

$$\underset{\text{Accumulation}}{\frac{\partial}{\partial t}(\varepsilon_k \rho_k \boldsymbol{v}_k)} + \underset{\text{Net rate of momentum outflow}}{\nabla \cdot (\varepsilon_k \rho_k \boldsymbol{v}_k \boldsymbol{v}_k)} = \underset{\text{External forces}}{\varepsilon_k \rho_k \boldsymbol{F}_k} + \underset{\text{Drag}}{\sum_{m=g,l,s} \beta_{km}(\boldsymbol{v}_m - \boldsymbol{v}_k)} + \underset{\text{Stresses}}{\nabla \boldsymbol{T}_k} \tag{3}$$

where $\beta_{km} = \beta_{mk}$ are the drag coefficients between the phases and $\boldsymbol{T}_k$ are the stress tensors.

The fluctuating energy (granular temperature) of the solids phase as derived in Gidaspow's book [25] is:

$$\frac{3}{2}\left[\underset{\text{Accumulation}}{\frac{\partial}{\partial t}\varepsilon_s \rho_s \theta} + \underset{\text{Net outflow of granular temperature, } \theta}{\nabla \cdot (\varepsilon_s \rho_s \boldsymbol{v}_s \theta)}\right] = \underset{\text{Production}}{\boldsymbol{T}_s : \nabla \boldsymbol{v}_s} + \underset{\text{Diffusion}}{\nabla \cdot \kappa_s \nabla \theta} - \underset{\text{Dissipation}}{\gamma_s} \tag{4}$$

where κ_s is the dense-phase granular conductivity for granular temperature and γ_s is the dissipation due to collision.

The gas phase energy balance as derived in Gidaspow's book [25] for model B is:

$$\underset{\text{Accumulation}}{\frac{\partial}{\partial t}(\varepsilon_g \rho_g H_g)} + \underset{\text{Net outflow}}{\nabla \cdot (\varepsilon_g \rho_g H_g \boldsymbol{v}_g)} = \underset{\text{Work due to gas pressure}}{\left(\frac{\partial P_g}{\partial t} + P_g \nabla \cdot \boldsymbol{v}_g\right)} + \underset{\text{Conduction}}{\nabla \cdot (k_g \nabla T_g)} + \underset{\text{Heat generation due to reaction}}{\sum_i r_{ig} \Delta H_{ig}} + \underset{\text{Phase change effects}}{\sum_{m=l,s} \{h_{vm}(T_m - T_g) + \beta_{gm}(\boldsymbol{v}_m - \boldsymbol{v}_g)^2\}} \tag{5}$$

Liquid and solids phase energy balances (k = l, s) are similar to the gas phase equation, except for the absence of the small pressures due to collisions:

$$\frac{\partial}{\partial t}(\varepsilon_k \rho_k H_k) + \nabla \cdot (\varepsilon_k \rho_k H_k \boldsymbol{v}_k) = h_{vk}(T_g - T_k) + \sum_{m=g,l,s} \beta_{km}(\boldsymbol{v}_m - \boldsymbol{v}_k)^2 + \nabla \cdot (k_k \nabla T_k) \tag{6}$$

Gas phase species balance with the assumption of negligible diffusion in the gas phase:

$$\underset{\text{Accumulation}}{\frac{\partial}{\partial t}(\varepsilon_g \rho_g y_g^j)} + \underset{\text{Net rate of outflow assuming each species moves with the gas phase velocity}}{\nabla \cdot (\varepsilon_g \rho_g y_g^j \boldsymbol{v}_g)} = \underset{\text{Production due reaction}}{\alpha^j \varepsilon_s \rho_s M^j r} \tag{7}$$

Constitutive equations are needed to close the above differential equation set. The most important contribution of the kinetic theory to the hydrodynamic model is the computation of the particulate viscosity. For the particulate phase, we use the granular flow theory invented by Savage and coworkers [32]. The viscosity is that found in the classical text, Chapman and Cowling, when one sets the ratio of Boltzmann constant to particle mass to unity and assumes a value of one for the restitution coefficient [25]. The restitution coefficient for the Air Products methanol catalyst was measured [33] to be close to 1. The expression we use for the viscosity was verified to give the viscosity measured by classical methods for gas–solid [34,35] and for liquid–solid [36] fluidization. The constitutive equations are as shown here.

Gas phase stress tensor—we use the Newtonian form without any artificial turbulence:

$$\boldsymbol{T}_g = -P_g \boldsymbol{I} + 2\varepsilon_g \mu_g \{\tfrac{1}{2}[\nabla \boldsymbol{v}_g + (\nabla \boldsymbol{v}_g)^T] - \tfrac{1}{3}(\nabla \cdot \boldsymbol{v}_g)\boldsymbol{I}\} \tag{8}$$

Liquid and solids phases stress tensor:

$$\boldsymbol{T}_k = (-P_k + \xi_k \nabla \cdot \boldsymbol{v}_k)\boldsymbol{I} + 2\mu_k\{\tfrac{1}{2}[\nabla \boldsymbol{v}_k + (\nabla \boldsymbol{v}_k)^{\mathrm{T}}] - \tfrac{1}{3}(\nabla \cdot \boldsymbol{v}_k)\boldsymbol{I}\} \quad (9)$$

Drag coefficient for gas and dispersed phases (for $\varepsilon_g \geq 0.8$)—for dilute flow, modified Stokes' law is used:

$$\beta_{gk} = \beta_{kg} = \frac{3}{4} C_D \frac{\rho_g \varepsilon_k |\boldsymbol{v}_g - \boldsymbol{v}_k|}{d_k} \varepsilon_g^{-2.65} \quad (10)$$

$$\begin{cases} C_d = \dfrac{24}{Re_k}(1 + 0.15 Re_k^{0.687}), & Re_k < 1000; \\ C_d = 0.44, & Re_k \geq 1000. \end{cases} \quad (11)$$

$$Re_s = \frac{\varepsilon_g \rho_g d_s |\boldsymbol{v}_g - \boldsymbol{v}_s|}{\mu_g} \quad (12)$$

Drag coefficient for gas and dispersed phases (for $\varepsilon_g < 0.8$)—for the dense-phase, the Ergun equation is used:

$$\beta_{gk} = \beta_{kg} = 150 \frac{(1-\varepsilon_g)\varepsilon_k \mu_g}{(\varepsilon_g d_k)^2} + 1.75 \frac{\rho_g \varepsilon_k |\boldsymbol{v}_g - \boldsymbol{v}_k|}{\varepsilon_g d_k} \quad (13)$$

Drag coefficient for dispersed phases:

$$\beta_{ls} = \beta_{sl} = \frac{3}{2}(1+e) \frac{\rho_s \rho_l \varepsilon_s \varepsilon_s |\boldsymbol{v}_l - \boldsymbol{v}_s|}{\rho_s d_s^3 + \rho_l d_l^3} (d_s + d_l)^2 \quad (14)$$

External forces acting on each phase:

$$\boldsymbol{F}_g = \frac{\boldsymbol{g}}{\varepsilon_g} \quad (15)$$

$$\boldsymbol{F}_k = \frac{\boldsymbol{g}}{\varepsilon_g} \left(1 - \frac{1}{\rho_k} \sum_{m=g,l,s} \varepsilon_m \rho_m\right) \quad (16)$$

Gas phase equation of state:

$$P_g = \rho_g \tilde{R} T_g \quad (17)$$

Enthalpy:

$$H_g = C_{pg}(T_g - T_g^0) \quad (18)$$

$$H_k = C_{pk}(T_k - T_k^0) \quad (19)$$

Constitutive equations for the solids phase—equation of state for particles:

$$P_s = \varepsilon_s \rho_s \theta [1 + 2(1+e) g_0 \varepsilon_s] \quad (20)$$

Bulk viscosity:

$$\xi_s = \frac{4}{3} \varepsilon_s^2 \rho_s d_s (1+e) g_0 \sqrt{\frac{\theta}{\pi}} \quad (21)$$

Solids viscosity:

$$\mu_s = \frac{2\mu_{s,dil}}{(1+e)g_0} \left[1 + \frac{4}{5}(1+e) g_0 \varepsilon_s\right]^2 + \frac{4}{5} \varepsilon_s^2 \rho_s d_s (1+e) g_0 \sqrt{\frac{\theta}{\pi}} \quad (22)$$

where

$$\mu_{s,dil} = \frac{5\sqrt{\pi}}{96} \rho_s d_s \sqrt{\theta} \quad (23)$$

Radial distribution function for the solids phase:

$$g_0 = \left[1 - \left(\frac{\varepsilon_s}{\varepsilon_{s,max}}\right)^{1/3}\right]^{-1} \quad (24)$$

Particles fluctuating energy conductivity:

$$\kappa_s = \frac{2\kappa_{dil}}{(1+e)g_0} \left[1 + \frac{6}{5}(1+e) g_0 \varepsilon_s\right]^2 + 2\varepsilon_s^2 \rho_s d_s (1+e) g_0 \sqrt{\frac{\theta}{\pi}} \quad (25)$$

where

$$\kappa_{s,dil} = \frac{75\sqrt{\pi}}{384} \rho_s d_s \sqrt{\theta} \quad (26)$$

Dissipation of the particles fluctuating energy:

$$\gamma = 3(1-e^2)\varepsilon_s^2 \rho_s g_0 \theta \left[\frac{4}{d_s}\sqrt{\frac{\theta}{\pi}} - \nabla \cdot \boldsymbol{v}_s\right] \quad (27)$$

where $e = 0.99999$ [33].

Gas–solid heat transfer: most correlations for solid-fluid heat transfer coefficients are of a power form of the Reynolds number. When used in computer codes there is a serious problem. When the Reynolds number goes to zero, there is no cooling. This gives absurd results. Hence, one adds a "2" to take care of the conduction effect. Gunn's [37] correlation does not have this defect. Hence, it is used in the code:

$$Nu_k = \left\{(2 + 5\varepsilon_k^2)(1 + 0.7 Re_k^{0.2} Pr^{1/3}) + \left(\frac{2}{15} + 1.2\varepsilon_k^2\right) Re_k^{0.7} Pr^{1/3}\right\} Sp_k \quad (28)$$

$$Nu_k = \frac{h_{vk} d_k}{k_g^0}, \qquad Pr = \frac{C_{p_g} \mu_g}{k_g^0}, \qquad Sp_k = \frac{6\varepsilon_k}{d_k} \quad (29)$$

Gas phase heat transfer:

$$k_g^0 = 8.65 \times 10^5 \left(\frac{T_g}{1400}\right)^{1.786} \quad (30)$$

$$k_g = \left(1 - \sqrt{1 - \varepsilon_g}\right) k_g^0 \quad (31)$$

Particulate phase heat transfer: we use an empirical equation employed by Syamlal and Gidaspow [38]. An alternate approach is to use an expression based on the kinetic theory:

$$\frac{k_k}{k_g^0} = \frac{\sqrt{\varepsilon_s}}{(1-\varepsilon_g)} \left\{\varphi \frac{k_k^*}{k_g^0} + (1-\varphi)\frac{k_k^0}{k_g^0}\right\} \quad (32)$$

$$\frac{k_k^0}{k_g^0} = \frac{2}{A_k}\left\{\frac{B_k\{k_k^*/k_g^0 - 1\}}{A_k^2(k_k^*/k_g^0)}\ln\left(\frac{k_k^*/k_g^0}{B_k}\right) - \frac{B_k - 1}{A_k} - \frac{B_k + 1}{2}\right\} \quad (33)$$

where

$$A_k = 1 - \left(\frac{B_k}{k_k^*/k_g^0}\right) \quad (34)$$

$$B_k = 1.25\left(\frac{\varepsilon_k}{\varepsilon_g}\right)^{10/9}(1 + 3\chi) \quad (35)$$

$$\chi = \sqrt{\frac{\left(\sum \varepsilon_k \rho_k\right)\left(\sum \varepsilon_k \rho_k / d_k^2\right)}{\left(\sum \varepsilon_k \rho_k / d_k\right)^2} - 1}, \quad k = \mathrm{l, s} \quad (36)$$

$$k_k^* = 0.3289, \qquad \varphi = 7.26 \times 10^{-3} \quad (37)$$

The only reaction considered in the simulation is the reaction between carbon monoxide and hydrogen to produce methanol:

$$CO + 2H_2 = CH_3OH \quad (38)$$

Several researchers had investigated the kinetic rate for methanol synthesis. There are two kinds of models, a power law rate expression model [39] and a mechanistic model [40]. A power law rate expression, discussed in Air Products' report [41] is used here. The model was based on the rate expression for methanol synthesis [42]:

$$r = \varepsilon_s \rho_s K_r f_{CO}^{1/3} f_{H_2}^{2/3}\left(1 - \frac{f_{MEOH}}{K_{eq} f_{CO} f_{H_2}^2}\right) \quad (39)$$

Model parameters were determined from experimental research:

$$K_r = 8.93 \times 10^{-3} \quad \text{and} \quad K_{eq} = \frac{6.249}{P^2} \quad (40)$$

To solve the set of transient partial differential equations earlier, we need appropriate initial and boundary conditions for the velocities of the three phases, the gas pressure, granular temperature and inlet and initial conditions for the chemical species. The operating conditions are the same as those of La Porte's RUN E-8.1 [41], where the slurry is not recirculated.

The gas volume fraction is set to one where particle-free gas enters the system. At the solid wall, the gas phase velocities in the two directions are generally set to zero. Since the particle diameter (50 μm) is smaller than the length scale of surface roughness of the rigid wall, a no slip boundary condition was assumed. For the granular temperature boundary conditions, we assume the energy flux at the wall to be zero. At the outlet, the pressure is the reactor pressure and the mass flux is assumed to be continuos. Mostofi [33] gives the detailed conditions (see Fig. 5).

4. La Porte pilot plant simulation

The heat exchangers in the Air Products/DOE La Porte slurry bubble column reactor were rearranged as shown in Fig. 4. The CFD code developed by Wu and Gidaspow [16] was used to simulate the methanol production in a similar but not identical manner as in Wu and Gidaspow [16]. Fig. 5 shows the simulation details and the initial conditions [33]. At start up, the solids concentration at the bottom of the reactor was assumed to be high, close to the minimum fluidization concentration. When the gas flow was turned on the initially high solids concentration flowed into the upper portion of the reactor. The continued flow of the reactant gas prevented the return of the catalyst into the lower stage. A CFD video of the simulation shows this phenomena. Unlike in the paper by Wu and Gidaspow [16], the whole column was simulated.

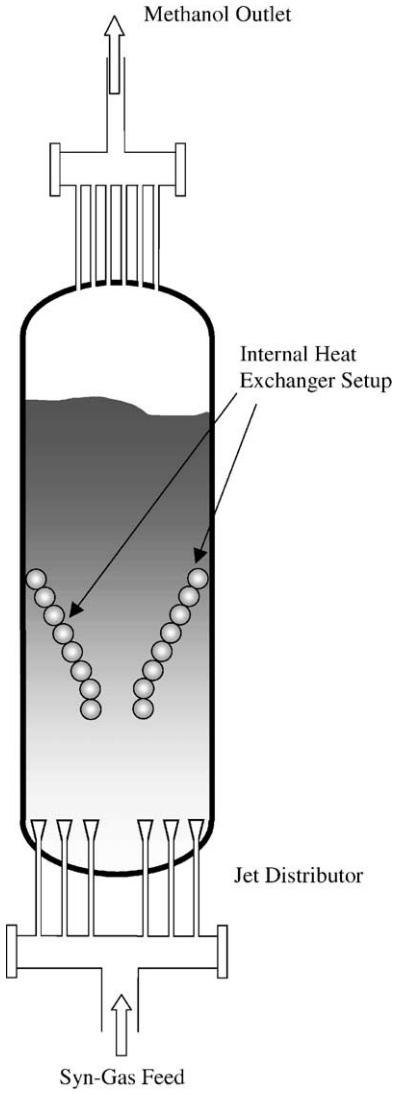

Fig. 4. Preferred heat exchanger arrangement in methanol slurry bubble column reactor.

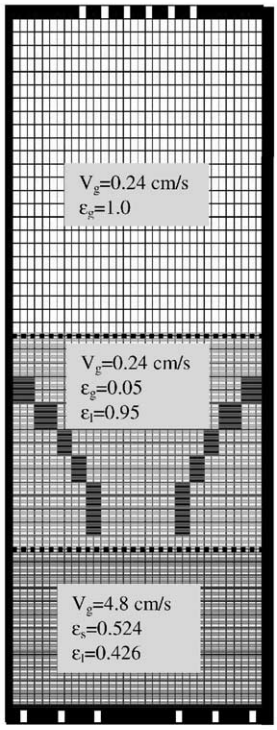

Inlet Conditions and System Properties	
Diameter of the reactor	61 cm
Height of the reactor	853 cm
Superficial gas velocity	15.24 cm/s
Temperature	250.3 °C
Pressure	753.2 psig
Catalyst diameter	50 μm
Restitution coefficient	0.99999
Liquid	wax
Density of liquid	0.70025 g/cm^3
Liquid Droplet Size	0.1 cm
Grid size (dx × dy)	1.79 × 20.3 cm
Number of cells in the grid	36 × 44
Time interval	10^{-5} sec
Initial Slurry Height	183 cm
Initial Liquid Height	427 cm

Initial Species Concentrations

	CO	CO2	H2	N2	CH3OH
% mol	51	13	35	1	0
y_g^j	68.07	27.26	3.34	1.33	0

Fig. 5. Slurry bubble column reactor simulation details and initial conditions.

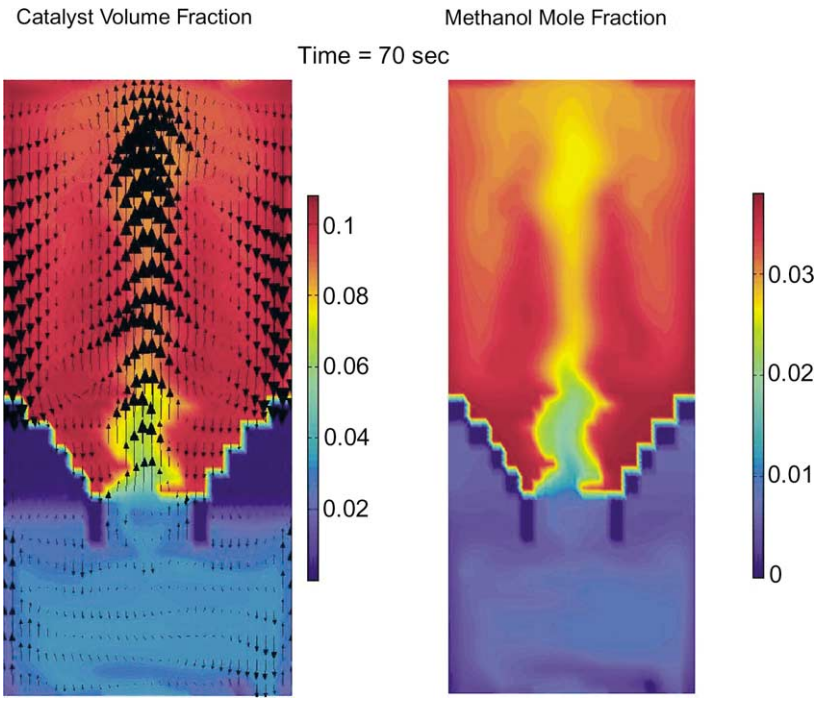

Fig. 6. Preferred reactor operation with high catalyst concentration in upper portion.

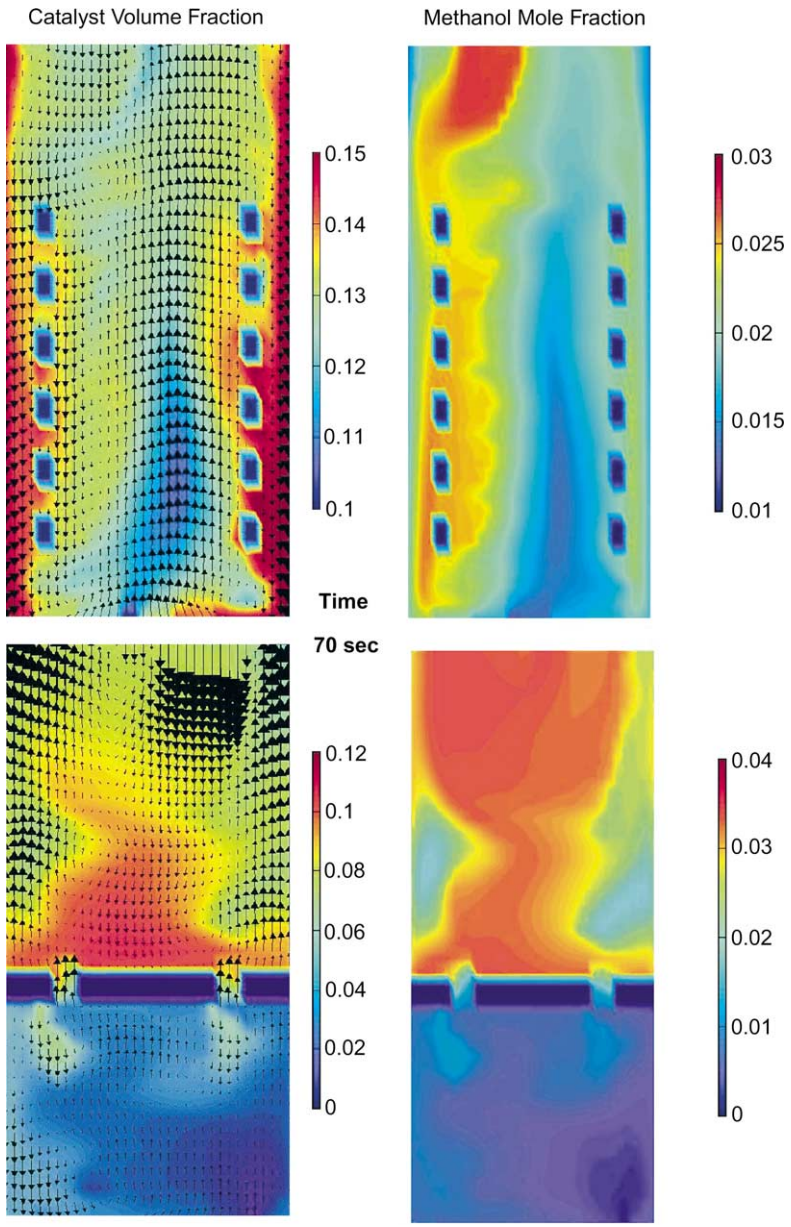

Fig. 7. A comparison of La Porte SBCR to an alternative staged reactor.

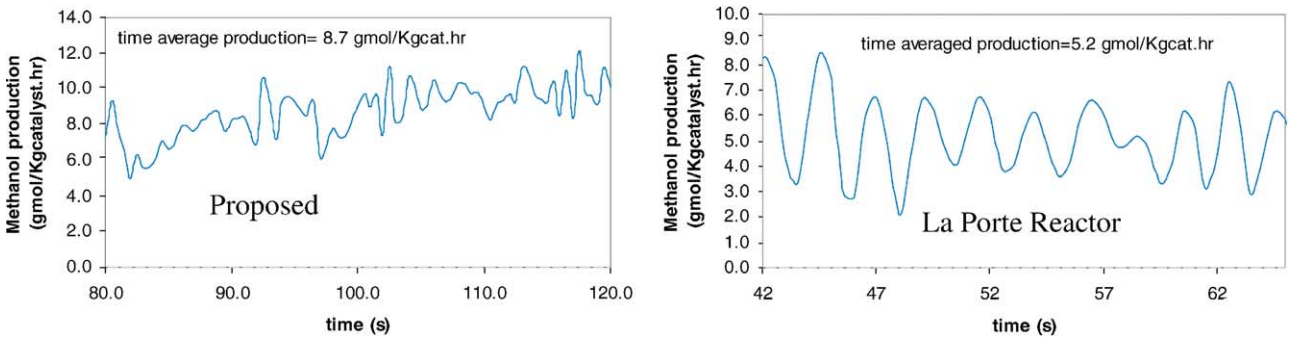

Fig. 8. A comparison of computed outlet methanol production of the La Porte reactor to the preferred configuration.

Fig. 6 shows the catalyst and the methanol distribution in the reactor at a time of 70 s. The concentration of the catalyst in the upper stage is higher than in the lower stage due to the fact that the catalyst is not allowed to return to the lower stage. The methanol concentration is higher in the upper stage due to the continued production and flow from the lower stage.

Fig. 7 shows a comparison of the La Porte SBCR to an alternative stage reactor concept. In the present La Porte reactor, the basic flow pattern is an upflow at the center and downflow at the walls. This type of a flow pattern mixes the product with the reactants at the bottom of the reactor and causes poorer production of products. In the stage reactor such mixing does not occur. The main reason however for a higher methanol production in a staged reactor is due to the highest catalyst concentration in the upper portion.

Fig. 8 shows the methanol production in the proposed configuration (Fig. 4) compared to that computed using the CFD model in the La Porte reactor. The methanol production reported here is based on that leaving with the gas only. The time averaged production for the proposed system is 8.7 g mol/h kg of catalyst versus 5.2 for the La Porte reactor. The methanol production for the staged configuration shown in Fig. 7 was computed to be 6.8 g mol/kg h.

5. Concluding remarks

Slurry bubble column reactors (SBCRs), such as those used to produce methanol and other liquids from synthesis gas, normally have a high catalyst concentration at the bottom of the reactor, when there is no liquid recirculation. Chang and Coulaloglu [43] of EXXON describe the disadvantages of such a catalyst distribution and suggest an improvement. Wu and Gidaspow [16] developed a CFD model for such process and compared the CFD results to the La Porte pilot plant methanol production runs. The CFD results show the unfavorable high solids concentration at the bottom of the reactor.

We have rearranged the heat exchangers in the La Porte unit and constructed a CFD model for a baffled reactor that has a higher concentration of the catalyst in the upper portion of the reactor. In this arrangement, the conversion to products is higher than in the La Porte unit, because there is more catalyst in the region of decreased reactant concentration. The baffled arrangement of the heat exchangers prevents the mixing of the catalyst from the upper stage, allowing continued operation of the reactor with a high concentration in the upper stage. Thus, an optimum catalyst concentration is maintained during the course of the production of the liquid fuels.

Acknowledgements

The authors are grateful to the referees for their useful comments, which helped improve the clarity of this manuscript. Dr. Gidaspow would like to acknowledge the partial financial support from the ORISE Faculty Research Participation Program.

References

[1] G.J. Stiegel, Liquid transportation fuels from coal. Part 2. Indirect liquefaction, PETC Review, PETC Office of Fossil Energy, US DOE, Issue 4, Fall, 1991.
[2] R.D. Srivastava, V.U.S. Rao, G. Cinquegrane, G.J. Stiegel, Catalysts for Fischer–Tropsch, Hydrocarbon Processing, February 1990, pp. 59–68.
[3] P.A. Ramachandran, R.V. Chaudhari, Three-Phase Catalytic Reactors, Gordon and Breach, New York, 1983.
[4] W.D. Deckwer, Bubble Column Reactors, Wiley, New York, 1992.
[5] L.-S. Fan, Gas–Liquid–Solid Fluidization Engineering, Butterworths, Boston, MA, 1989.
[6] A. Prakash, P.B. Bendale, Vikings System International, Design of Slurry Reactor for Indirect Liquefaction Applications, Report to DOE/PETC, DE-AC22-89PC89870.
[7] G.P. Van der Laan, A.A.C.M. Beenackers, R. Krishna, Multicomponent reaction engineering model for Fe-catalyzed Fischer–Tropsch synthesis in commercial scale slurry bubble column reactors, Chem. Eng. Sci. 54 (1999) 5013–5019.
[8] S. Degaleesan, M.P. Dudukovic, B.A. Toseland, B.L. Bhatt, A Two-compartment convective-diffusion model for slurry bubble column reactors, Ind. Eng. Chem. Res. 36 (1997) 4670–4680.
[9] B.L. Tarmy, C.A. Coulaloglu, Alpha-omega and beyond industrial view of gas/liquid/solid reactor development, Chem. Eng. Sci. 47 (1992) 3231–3246.
[10] Y. Pan, M.P. Dudukovic, M. Chang, Numerical investigation of gas-driven flow in 2-D bubble columns, AIChE J. 46 (3) (2000) 434–449.
[11] M.P. Dudukovic, Opaque multiphase flows: experiments and modeling, Keynote lecture, in: Proceedings of the International Conference on Multiphase Flows, New Orleans, LA, 27 May–1 June 2001.
[12] X.L. Luo, D.J. Lee, R. Lau, G. Yang, L.-S. Fan, Maximum stable bubble size and gas holdup in high-pressure slurry bubble columns, AIChE J. 45 (4) (1999) 665–680.
[13] D. Mitra-Majumdar, B. Farouk, Y.T. Shah, Hydrodynamic modeling of three-phase flows through a vertical column, Chem. Eng. Sci. 52 (24) (1997) 4485–4497.
[14] M.S. Bohn, First 3-D simulation of bubble column hydrodynamics paves way for commercial gas-to-liquid conversion in slurry reactor, Technical Publications of Rentech Inc., from www.rentechinc.com, 2000.
[15] D. Matonis, D. Gidaspow, M. Bahary, CFD simulation of flow and turbulence in a slurry bubble column, AIChE J. 48 (7) (2002) 1413–1429.
[16] Y. Wu, D. Gidaspow, Hydrodynamic simulation of methanol synthesis in gas–liquid slurry bubble column reactors, Chem. Eng. Sci. 55 (2000) 573–587.
[17] W.D. Deckwer, A. Schumpe, Improved tools for bubble column reactor design and scale-up, Chem. Eng. Sci. 48 (1993) 889–911.
[18] M. Bahary, Experimental and computational studies of hydrodynamics of three-phase and two-phase fluidized beds, Ph.D. Thesis, Illinois Institute of Technology, Chicago, 1994.
[19] S.L. Soo, Fluid Dynamics of Multiphase Systems, Blaisdell, Waltham, MA, 1967.
[20] R. Jackson, Hydrodynamic stability of fluid-particle systems, in: J.F. Davidson, R. Cliff, D. Harrison (Eds.), Fluidization, Academic Press, New York, 1985, pp. 47–72.
[21] R.M. Bowen, Theory of mixtures, in: A.C. Eringen (Ed.), Continuum Physics, vol. III, Academic Press, New York, 1976.

[22] J.X. Bouillard, D. Gidaspow, Porosity distribution in a fluidized bed with an immersed obstacle, AIChE J. 35 (1989) 908–922.
[23] I. Gamwo, K.Y. Soong, D. Gidaspow, R.W. Lyczkowski, Three-dimensional hydrodynamic modeling of a bubbling fluidized bed, in: Proceedings of the 13th International Conference on Fluidized Bed Combustion, vol. 1, ASME, New York, 1995, p. 297.
[24] U.K. Jayaswal, Hydrodynamics of multiphase flows: separation, dissemination and fluidization, Ph.D. Thesis, Illinois Institute of Technology, Chicago, 1991.
[25] D. Gidaspow, Multiphase Flow and Fluidization: Continuum and Kinetic Theory Descriptions, Academic Press, New York, NY, 1994.
[26] I. Gamwo, K.Y. Soong, R.W. Lyczkowski, Numerical simulation and experimental validation of solids flows in a bubbling fluidized bed, Powder Technol. 103 (1999) 117–129.
[27] F.H. Harlow, A. Amsden, A numerical fluid dynamics calculation method for all flow speeds, J. Comput. Phys. 8 (1971) 197–213.
[28] W.C. Rivard, M.D. Torrey, K-FIX: a computer program for transient two-dimensional, two-fluid flow, LA-NUREG-6623, Los Alamos, 1977.
[29] H.B. Stewart, B. Wendroff, Two-phase flow: models and methods, J. Computat. Phys. 56 (1984) 363–409.
[30] R. Pape, D. Gidaspow, Numerical simulation of intense reaction propagation in multiphase systems, AIChE J. 44 (1998) 294–309.
[31] R.W. Lyczkowski, D. Gidaspow, C.W. Solbrig, E.C. Hughes, Characteristics and stability analysis of transient one-dimensional two-phase flow equations and their finite difference aproximations, Nucl. Sci. Eng. 66 (1978) 378–396.
[32] C.K. Lun, S.B. Savage, D.J. Jeffrey, N. Chepurniy, Kinetic theory for granular flow: inelastic particles in Couette flow and slightly inelastic particles in a general flow field, J. Fluid Mech. 140 (1984) 223–256.
[33] R. Mostofi, CFD simulations of particulate two-phase and three-phase flows, Ph.D. Thesis, Illinois Institute of Technology, Chicago, 2002.
[34] D. Gidaspow, L. Huilin, Collisional viscosity of FCC particles in a CFB, AIChE J. 42 (1996) 2503–2510.
[35] Y.A. Buyevich, G.D. Cody, Particle fluctuations in homogeneous fluidized beds, in: Proceedings of the Brighton World Congress on Particle Technology, vol. 3, Paper 207, Brighton, UK, 1998.
[36] D. Gidaspow, L. Huilin, Equation of state and radial distribution functions of FCC particles in a CFB, AIChE J. 44 (1998) 279–293.
[37] D.J. Gunn, Transfer of heat or mass to particles in fixed and fluidised beds, Int. J. Heat Mass Trans. 21 (1978) 467–476.
[38] M. Syamlal, D. Gidaspow, Hydrodynamics of fluidization: prediction of wall to bed heat transfer coefficients, AIChE J. 31 (1985) 127–135.
[39] V.W. Wedel, S. Ledakowicz, W.D. Deckwer, Kinetics of methanol synthesis in the slurry-phase, Chem. Eng. Sci. 43 (1998) 2169–2174.
[40] S. Lee, Methanol Synthesis Technology, CRC Press, Boca Raton, 1990.
[41] Air Products and Chemicals Inc., Liquid Phase Methanol La Porte Process Development Unit: Modification, Operation, and Support Studies, Draft Report to DOE for Contract No. DE-AC22-90PC89865, 1991.
[42] F.R. Weimer, M.D. Terry, P.R. Stepanoff, Laboratory kinetics and mass transfer in the liquid phase methanol process, in: Proceedings of the AIChE National Meeting, New York, 1987.
[43] M. Chang, C.A. Coulaloglou, Enhanced catalyst mixing in slurry bubble columns, US Patent 5252613 (1993).